

# Coherence interpretation of the delayed-choice quantum eraser

Sangbae Kim and Byoung S. Ham\*

Center for Photon Information Processing, and School of Electrical Engineering and Computer Science,  
Gwangju Institute of Science and Technology, 123 Chumdangwagi-ro, Buk-gu, Gwangju 61005, South  
Kore; bham@gist.ac.kr

\* Correspondence: bham@gist.ac.kr; Tel.: +82-62-715-3502

Received: October 31, 2022

**Abstract:** Quantum superposition is the cornerstone of quantum mechanics, where interference fringes originate in the self-interference of a single photon via indistinguishable photon characteristics. Wheeler's delayed-choice experiments have been extensively demonstrated over the last decades to understand the complementarity theory of quantum mechanics for the wave-particle duality. The heart of the delayed-choice experiments is in the mutually exclusive quantum feature violating the cause-effect relation. Here, we experimentally demonstrate the violation of the cause-effect relation using coherent photons for the quantum eraser. Unlike most delayed-choice schemes using undetermined photons in MZI, the present scheme is for the determined photon for the MZI via post-measurement controls. The observed quantum eraser is coherently interpreted to seek the origin of the cause-effect violation.

**Keywords:** quantum coherence; quantum eraser; quantum mechanics

## 1. Introduction

The quantum superposition-related delayed-choice experiments proposed by Wheeler in 1978 [1], which is based on Heisenberg's uncertainty principle and Bohr's complementarity theory [2], have been intensively studied over the last several decades [3-17]. The delayed-choice experiment in a Mach-Zehnder interferometer (MZI) represents an intrinsic quantum feature of the wave-particle duality of a photon or particle [3]. This quantum phenomenon shows a trade-off relation between the wave nature-based fringe visibility and particle nature-based which-way information [4]. Such a quantum feature has been broadly demonstrated using thermal lights [5], entangled photons [6-10], atoms [11-13], neutrons [3], attenuated laser [4,14,15], and antibunched photons [16].

In the Wheeler's delayed-choice experiments, a post-control of measurements results in a paradoxical phenomenon between the wave and particle natures [17]. Here, the post-control normally represents a classical control of the MZI itself to retrospectively determine undetermined photon characteristics inside the MZI. A quantum version of the delayed-choice experiments has also been presented by replacing the classical control unit with a quantum device, resulting in quantum superposition between the wave and particle natures of a single photon [14,16]. Thus, the delayed-choice experiments have shown an intrinsic quantum property of complementarity between the particle and wave natures of a single photon, where the single photon can be either a thermal, coherent, or quantum particle [17].

In the present Article, the delayed-choice experiment is differently conducted using coherent photons for the quantum eraser via post-measurements of the output photon's polarization basis. Unlike most delayed-choice schemes limited to the direct control of MZI, the present scheme is not for the MZI itself but for the output photon's polarization basis. On the contrary of the most delayed-choice experiments with an undetermined photon nature, the present one is for a pre-determined photon having the particle nature, where the post-measurement control retrospectively reverses it into the wave nature. Here, our MZI is composed of a polarizing beam splitter (PBS) and a beam splitter (BS), satisfying the criteria of the particle nature according to the Fresnel-Arago law [18]. Thus, the which-way information of the photon inside the MZI is predetermined, resulting in no interference fringe.

Without controlling the MZI itself, we experimentally demonstrate the quantum eraser via post-measurements of the output photon's polarization basis projection. The observed quantum eraser is interpreted coherently to understand the quantum mystery.

## 2. Experimental setup for the quantum eraser

Figure 1 shows schematic of the present delayed-choice quantum eraser using a coherent photon generated from an attenuated laser. For single photon measurements, a coincidence counting unit (CCU, DE2; Altera) is used to count single-photon measurements from both single photon detectors D1 and D2 (SPCM-AQRH-15, Excelitas). The generation ratio of Poisson-distributed multi-photons is adjusted to be negligible less than 1 % of single photons. For the polarization basis randomness of the input photon, the vertically polarized light is 22.5°-rotated by a half-wave plate (HWP) to produce a superposition state  $|\psi\rangle_{HWP}$ :  $|\psi\rangle_{HWP} = \frac{1}{\sqrt{2}}(|V\rangle + |H\rangle)$ . By the followed PBS, the superposed state is appeared as the particle nature inside the MZI with complete distinguishability:  $|\psi\rangle_{UP} = |V\rangle$ ;  $|\psi\rangle_{LP} = |H\rangle$ .

Due to this distinguishable photon characteristics, the MZI has no  $\varphi$ -dependent interference fringe in measurements of output photons ( $E_1; E_2$ ) before the polarizers Ps in Fig. 1. This is due to the Fresnel-Arago law [18], satisfying the preset which-way information by the PBS in Fig. 1. Unlike the assumption of conventional delayed-choice experiments, thus, the photon characteristic is predetermined for the particle nature of quantum mechanics. Now, our discussion focuses on the violation of this predetermined particle nature by measurements of the output photons without control of the MZI system. For the polarization distinguishable photons, refs. [15, 19] are closest to the present model. Unlike ref. 19 based on paired entangled photons, however, Fig. 1 uses a single photon from an attenuated laser as in ref. [15]. A fixed phase relation in an entangled photon pair has been demonstrated theoretically [20] and experimentally [21,22]. As discussed later, thus, the entangled photons in ref. 19 also satisfy the MZI system of Fig. 1. Due to the classical physics rooted in the cause-effect relation, the action of Ps placed outside MZI cannot change the MZI property in a time reversed manner because it does not influence the photon inside the MZI. If this fact is violated, the measurements belong to the quantum mystery of the delayed-choice quantum eraser [17].

For the projection measurement control of the output photon in Fig. 1, each MZI output photon passes through a polarizers P, whose rotation angle  $\theta$  is given with respect to the vertical axis  $\hat{y}$ . The input field  $E_0$  denotes an amplitude of a single photon achieved from an attenuated laser L, whose mean photon number is set at  $\langle n \rangle \sim 0.01$ , satisfying the incoherence condition between consecutive single photons (see Appendix A). In other words, the post-measurements are for a statistical ensemble of independent particles having distinguishable photon characteristics of  $|\psi\rangle_{PBS}$ . For this, the laser L is chosen to be ultrawide ( $\sim$ THz) in its spectral width at wavelength  $\lambda = 532$  nm, such that the mean distance (600 m) between consecutive photons is to be far greater than the coherence length  $l_c$  ( $\sim$ 3 mm) of the laser L. Here, the coherence length determines the physical size of the wave packet of the measureable single photons.

For the projection measurements in Fig. 1, singe photon detectors (D1, D2) are used as input sources in the typical set-up of coincidence detection by CCU. For the MZI phase control  $\varphi$ , the path-length difference ( $\Delta L$ ) is adjusted far less than the coherence length  $l_c$ . This coherence satisfaction for the wave nature is easily tested with the same polarized photon-based MZI interference. Thus, the MZI in Fig. 1 satisfies a general scheme of single-photon (noninterfering) interferometer, whose purpose is whether the violation of the cause-effect relation occurs or not by the output photon's polarization control.

Each output photon ( $E_1$  or  $E_2$ ) from the MZI is denoted as a superposition state of the orthonormal polarization bases at equal probability amplitudes:  $|\psi\rangle_{out} = \frac{1}{\sqrt{2}}(|V\rangle + |H\rangle) = |\psi\rangle_{HWP}$ . This polarization-basis randomness of the MZI output photons is originated in the random polarization bases by the 22.5°-rotated HWP. Due to the orthogonally polarized photons, the photon characteristic inside the

MZI is predetermined as the particle nature, resulting in no interference fringe in each output port. Thus, we now focus on the post-control of the MZI output photons via polarization projections onto a rotated polarizer  $P$  (see Inset of Fig. 1). This scheme is similar to refs. 15, 19 and 22, where the distinguishable photon characteristics are satisfied by a wave plate (or polarizer) placed inside the MZI. Even though two sets of entangled photon pairs are superposed in refs. 19 and 22, the same MZI set-up provided by the fixed phase between the photon pairs, results in path-polarization distinguishability.

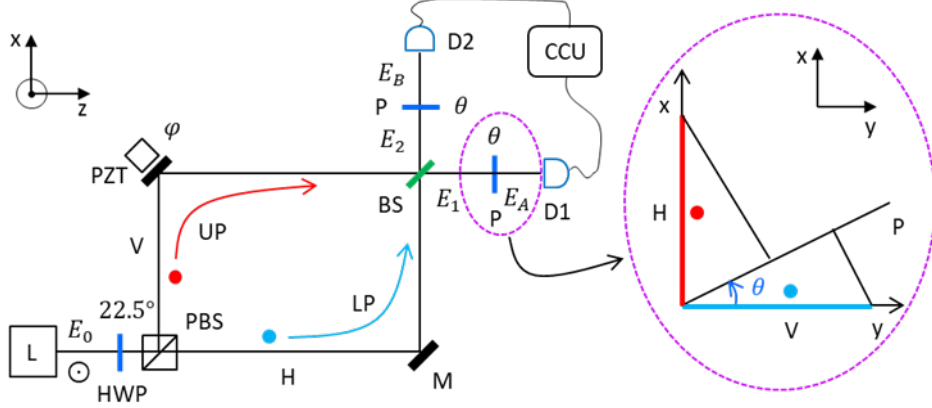


**Figure 1.** Schematic of the quantum eraser. (Dotted circle) Projection onto a polarizer. L: laser, HWP: half-wave plate, PBS: polarizing beam splitter, H (V): horizontal (vertical) polarization, M: mirror, PZT: piezo-electric transducer, BS: beam splitter, P: polarizer, D1/D2: single photon detector. CCU: coincidence counting unit. The light of laser L is vertically polarized with respect to the plane of incidence. Each colored dot indicates a single photon having the same probability amplitude.

### 3. Analytical results

To coherently interpret the delayed-choice quantum eraser in Fig. 1, the MZI of Fig. 1 is analyzed using coherence optics for the output photons:

$$\begin{bmatrix} E_1 \\ E_2 \end{bmatrix} = \frac{E_0}{2} [BS][\Phi][PBS][HWP] \begin{bmatrix} 1 \\ 0 \end{bmatrix} \\ = \frac{E_0}{2} \begin{bmatrix} i(H + Ve^{i\varphi}) \\ H - Ve^{i\varphi} \end{bmatrix}, \quad (1)$$

where  $[BS] = \frac{1}{\sqrt{2}} \begin{bmatrix} 1 & i \\ i & 1 \end{bmatrix}$ ,  $[\Phi] = \begin{bmatrix} 1 & 0 \\ 0 & e^{i\varphi} \end{bmatrix}$ ,  $[PBS][HWP] = \begin{bmatrix} H & iV \\ iV & H \end{bmatrix}$ , and  $E_0$  is the amplitude of a single photon. Here, V (H) represents a unit vector of vertically (horizontally) polarized photon. Most importantly, interference between the H- and V-polarized photons on the BS of the MZI shows independent photon characteristics in both output ports. Thus, the calculated intensities of  $E_1$  and  $E_2$  in Eq. (1) are  $I_1 = I_2 = I_0/2$ , regardless of  $\varphi$ . This is the first result of the predetermined photon nature inside the MZI, demonstrating the particle nature of quantum mechanics for the input photon  $E_0$ .

By inserting a polarizer ( $P$ ) in each output path of the MZI, Eq. (1) is rewritten as (see Inset of Fig. 1):

$$E_A = \frac{iE_0}{2} (\sin\theta + \cos\theta e^{i\varphi}), \quad (2)$$

$$E_B = \frac{E_0}{2} (\sin\theta - \cos\theta e^{i\varphi}), \quad (3)$$

where  $\theta$  is the rotation angle of  $P$  with respect to its vertical axis. Thus, Eqs. (2) and (3) represent polarization projections of the output photon onto the  $P$  axis rotated by an angle  $\theta$ , resulting in polarization-basis transformation:  $\hat{V} \rightarrow \hat{P}\cos\theta$  and  $\hat{H} \rightarrow \hat{P}\sin\theta$ . Here, the positive  $\theta$  is for the clockwise

direction from the vertical axis (y) of the photon propagation direction (z) (see the Inset of Fig. 1). For the negative rotation, however, the projections are denoted by  $\hat{V} \rightarrow \hat{p}\cos\theta$  and  $\hat{H} \rightarrow -\hat{p}\sin\theta$ . The projection results onto the polarizer P represent the post-measurements of the MZI.

The calculated intensities of Eqs. (2) and (3) are as follows:

$$I_A = \frac{I_0}{4}(1 + \sin 2\theta \cos \varphi), \quad (4)$$

$$I_B = \frac{I_0}{4}(1 - \sin 2\theta \cos \varphi), \quad (5)$$

where the orthogonal basis product is now allowed by the basis transformation. Equations (4) and (5) are the second result of the present research for the quantum eraser whose origin is in the photon coherence.

For  $\theta = \pm \frac{\pi}{4}$  ( $\pm 45^\circ$ ), Eqs. (4) and (5) are rewritten as:

$$I_A = \frac{I_0}{4}(1 \pm \cos \varphi), \quad (6)$$

$$I_B = \frac{I_0}{4}(1 \mp \cos \varphi). \quad (7)$$

For Eqs. (6) and (7), the local randomness of the P-projected photons demonstrated in ref. 22 can also be satisfied here in Fig. 1 by combining both  $\theta$  bases, where  $\theta \in \{-45^\circ, +45^\circ\}$ . This is the fundamental difference between coherent photon and entangled photon pair, where the entangled photons are produced via spatial mixing of the signal and idler photons [23]. The sum of the polarization bases in Eqs. (6) and (7) corresponds to the entangled photon-pair case of the second-order ( $\chi^{(2)}$ ) nonlinear optical process. Two-photon correlation between Eqs. (6) and (7) shows a fringe regardless of the local realism, as demonstrated in refs. [19,22], if the sign correlation between Eqs. (6) and (7) can be kept for measurements. Regarding the causality violation, Eqs. (6) and (7) witness the quantum feature of the delayed-choice quantum eraser for Fig. 1.

### 3. Experimental results

The measurements for both output photons from the MZI in Fig. 1 are conducted by CCU via a set of single photon detectors D1 and D2 (see Fig. 2). The dead time and dark count rate of the single photon detectors are 22 ns and 50 counts/s, respectively. The resolving time of the single photon detector is  $\sim 350$  ps, whose generated electrical pulse duration is  $\sim 6$  ns. For the polarization projection by Ps in Figs. 1 and 3, four different rotation angles are set (-45, 0, 45 or 90 degrees) to the clockwise direction with respect to the vertical axis of the light propagation direction. The photon counts in Figs. 2 and 4 are measured by CCU for 0.1 s and calculated by a home-made Labview program.

In Fig. 1, the laser L is SDL-532-500T (Shanghai Dream Laser), whose center wavelength and coherence length are 532 nm and 3 mm, respectively. The laser light is vertically polarized. For the random but orthogonal polarizations of a single photon, a half-wave plate (HWP) is rotated by 22.5 degrees from its fast axis. For a single photon, the laser L is attenuated by neutral density filters, satisfying Poisson distribution (see Appendices A and B). For Figs. 2 and 5, the mean photon number is set at  $\langle n \rangle \sim 0.01$ . The maximum number of measured single photons in each MZI output port is  $\sim$  a half million per second (see Fig. 2), resulting in the mean photon-to-photon distance of 600 m. Compared with the laser's coherence length, it is clear that the measured photons are completely independent and incoherent among them. On behalf of the polarizing beam splitter (PBS), perpendicularly and horizontally polarized components of an incident photon are separated into the upper (UP) and lower paths (LP), respectively. Both split components of a single photon are recombined in the beam splitter BS, resulting in PB (PBS-BS)-MZI. Thus, the photons in the PB-MZI in Fig. 1 act as particles, resulting in no interference fringes in the output ports. Thus, the photon property of the particle nature inside the MZI is confirmed.

The length of each path of the PB-MZI is set at 2 m, and the path-length difference between UP and LP is kept to be far less than 3 mm to satisfy the coherence condition. This coherence condition is essential for the delayed-choice experiments. The  $\varphi$  phase control of the PB-MZI is conducted by a piezo-electric optic mount (PZT; KC1-PZ, Thorlabs) connected by a PZT controller (MDT693A, Thorlabs) and a function generator (AFG3021, Tektronix). For Figs. 2 and 5, the data is measured under

the  $\varphi$  scanning mode, where the phase resolution is  $\frac{2\pi}{180}$  radians. Thus, Figs. 2 and 5 have 180 data points for a  $2\pi$  cycle of  $\varphi$  (see Table 1 of Appendix A). The BS position for recombination of two split components of a single photon is well adjusted for a complete overlap between them.

The upper and middle panels of Fig. 2 show the experimental data of single photons measured by D1 and D2, respectively, for different  $\theta$ s. As expected from Eqs. (6) and (7), fringes appear in both measurements for  $\theta = \pm 45^\circ$ . However, no fringes appears for  $\theta = 0^\circ; 180^\circ$ , as expected by Eqs. (4) and (5) (see the overlapped green and black lines). The observed fringes represent the wave nature of the photon inside the MZI in Fig. 1. As shown in Appendices A and B, the statistical error (standard deviation) in single photon measurements is less than 1 %. This is a big benefit of using coherent photons from a stabilized laser compared to entangled photons from spontaneous parametric down conversion process (SPDC) [19]. Because the PB-MZI is not actively stabilized, most errors are from the air turbulence affecting MZI path lengths.

The observed fringes in Fig. 2 demonstrate the same mysterious quantum eraser in terms of the reversed order in measurements, because the predetermined particle nature of the photon inside the MZI (see the green line) cannot be controlled or changed by the post-measurements of the output photons [14]. If the coherence condition between UP and LP is broken by adjusting the path-length difference ( $\Delta L$ ) to exceed the coherence length ( $l_c$ ) of the photon ( $\Delta L \gg l_c$ ), no fringe is observed for any  $\theta$ s, as shown in the bottom panel (see also Appendix C). Thus, the coherence of the photon is the bedrock of the delayed-choice quantum eraser. This fact has never been clearly discussed before. Thus, the quantum eraser has been successfully demonstrated with coherence approach. This is the third result of the present delayed-choice quantum eraser.

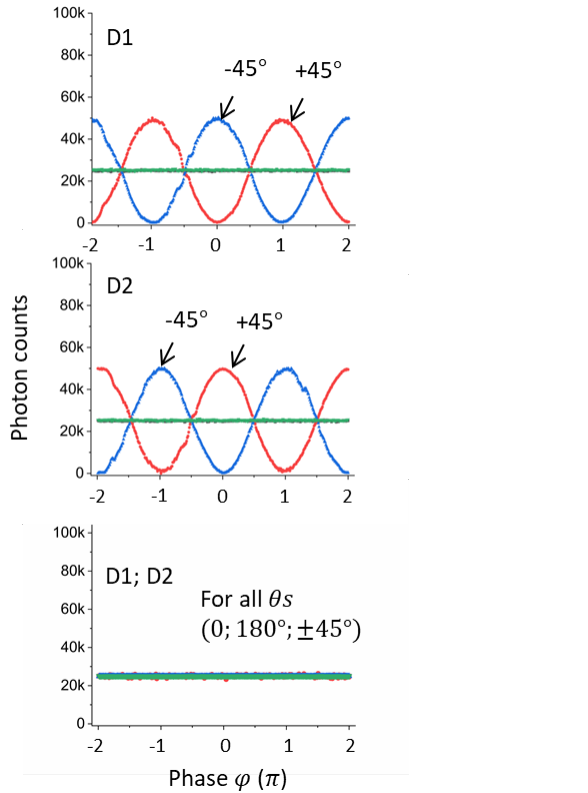


**Figure 2.** Experimental observations of the delayed-choice quantum eraser. Red:  $\theta = 45^\circ$ , Blue:  $\theta = -45^\circ$ , Green:  $\theta = 0^\circ$ , Black:  $\theta = 180^\circ$ . (Top and middle)  $\Delta L \ll l_c$ , where  $\Delta L$  is path-length difference between UP and LP.  $l_c$  is coherence length of the laser L. (Bottom)  $\Delta L \gg l_c$ . Photon counts are for 0.1 s. Total data points for each  $\theta$  in each panel are 360. The measured statistical error in each data is less than 1 % (see Appendix B).

#### 4. Discussion

It is the well-known fact that the most mysterious phenomenon in quantum mechanics is quantum superposition as Feynman mentioned [24]. Figure 3(a) shows a corresponding scheme to Fig. 1, where each output of the MZI in Fig. 1 are the superposition of orthogonal polarization bases with the same probability amplitudes. Figure 3(b) is an interferometric version of Fig. 3(a), where the second BS-caused phase shift ( $\pi/2$ ) [25] can be controlled by  $\varphi$  adjustment. In Fig. 3(a), the split photon by BS satisfies quantum superposition between two paths of UP and LP by the same probability amplitude of polarization basis. By the 90-degree rotation of polarization of a photon in UP, the superposition of orthogonal polarization bases on the second BS in Fig. 3(b) is equal to that in Fig. 1(a). Then, one of the output ports is measured for polarization projection by using a rotated polarizer P. The causality violation is tested whether the  $\varphi$ -dependent interference fringe occurs. Thus, Fig. 3(b) is equivalent to Fig. 1, resulting in the delayed-choice quantum eraser [19].

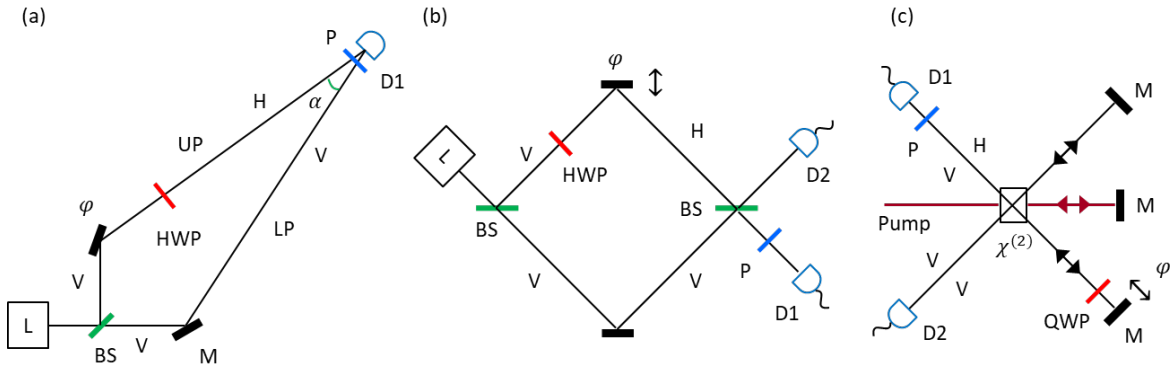


**Figure 3.** Equivalent schemes. (a) Classical beating-based. (b) MZI-based corresponding to (a). (c) Entangled photon-based corresponding to (a) (see ref. 19). QWP: quarter-wave plate.

Figure 3(c) shows the experimental scheme of the delayed-choice quantum eraser using an entangled photon-based double-pass scheme, where the entangled photon pairs are probabilistically superposed by the consecutive action of the forward and backward pump photons [19]. Like Fig. 3(a), first entangled photons by the forward pump in Fig. 3(c) are vertically (V) polarized. By an inserted quarter wave plate (QWP) in one path, however, orthogonal polarization superposition is resulted at D1 detector along with the backward pump-generated entangled photon pair. Due to the 90-degree phase shift between entangled photons [20,21], there is no fundamental difference between Figs. 3(b) and (c) in terms of polarization superposition in both detectors, where the function of HWP in Fig. 3(b) is the same as QWP in Fig. 3(c). Whether the light source is classical (coherent; Poissonian; thermal) or quantum (entangled; sub-Poissonian; squeezed), the basis superposition in Fig. 3 represents for independent (polarization basis) entities, i.e., the particle nature of a photon. Unlike classical independence, however, the superposed polarization bases of a single (or entangled) photon must be coherent, as demonstrated in Fig. 2. This coherent basis randomness is equivalent to indistinguishability in quantum superposition. Unlike classical independence, thus, coherence between the paired bases (entities) must be assumed in quantum superposition, even though this fact is not specified.

Figure 4(a) shows details of the experimental configuration of Fig. 3(a). The longitudinal distance between M2 and the slit S is 2 m. Figures 4(b) and (c) are the images captured by a CMOS camera placed M2 and S, respectively. In Fig. 4(b), the smallest separation (transverse distance, d) between two beams (UP, LP) is obtained by using a D-shaped mirror (M2), where the separation 'd' between UP and LP is nearly diffraction limited at  $\sim 200$   $\mu$ m. Figure 4(c) shows the image of the spatial interference fringe on the position S caused by the d-separated two beams. For the single photon data in Fig. 4, only a center

fringe (see the box in Fig. 4(c)) is taken through the slit S (see the box in the image). The images of Figs. 4(b) and (c) are for continuous wave of laser L.

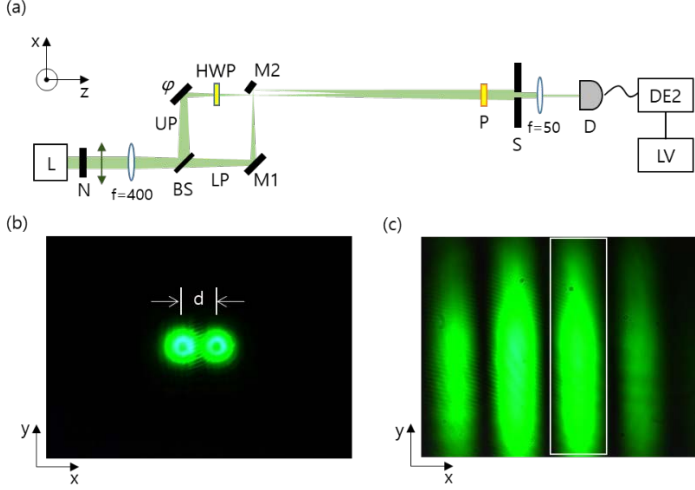


**Figure 4.** Schematic of Fig. 3(a). (a) Detailed configuration of Fig. 3(a). L: laser, N: neutral density filter, BS: beam splitter,  $\varphi$ (PZT): piezo-electric transducer, HWP: half-wave plate, M1: mirror, M2: D-shaped mirror, P: polarizer, S: slit, D: single photon detector (or avalanche photon diode). (b) Image of two beams (LP and UP) right after M2. (c) Image of interference fringe on the position S.

Figure 5(a) shows experimental results of Fig. 4(c) with single photons for four different rotation angles of P as a function of  $\varphi$ . For this, the center fringe of Fig. 4(c) is filtered out through a homemade slit to the single photon detector D. Thus, the captured photon number is severely reduced compared with Fig. 2. As shown in Fig. 5(a), the polarizer's rotation angle  $\theta$  gives the same effect as in Fig. 2, resulting in the same causality violation (see also Eqs. (6) and (7)). Unlike conventional delayed-choice experiments [17], the pre-determined photon characteristic has been retrospectively controlled via post-measurement control of the polarization basis, as in ref. [15,19,22]. Figure 5(b) is for the same polarizers without HWP, resulting in no causality violation. This is due to the preset wave nature of photons for the same polarization basis. Thus, Fig. 5(b) follows normal coherence optics of coherent superposition:  $E_s = E_{UP} + E_{LP}$ ;  $I_s = I_0(1 \pm \cos\varphi)$ . Here, the action of P in Fig. 5(b) simply reduces the observed photon counts into a half for  $\theta = \pm 45^\circ$ .

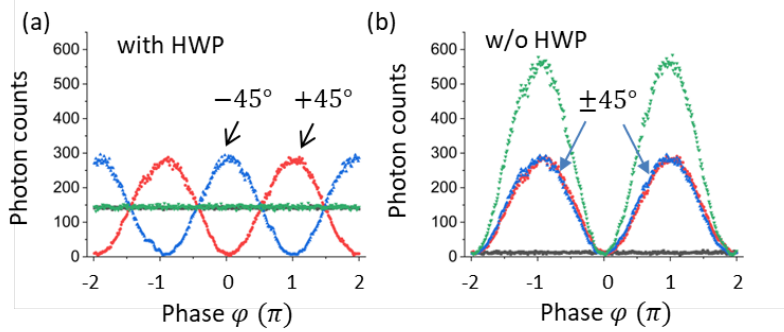


**Figure 5.** Experimental demonstrations for FIG. 4(a). (a) With HWP. (b) Without HWP. The single photon counts are for 0.1 s. Rotation angle  $\theta$  of the polarizer P: Blue ( $-45^\circ$ ), Red ( $45^\circ$ ), Green ( $0^\circ$ ), Black  $180^\circ$ .

Unlike Fig. 5(b), Fig. 3(c) results in no fringe without QWP due to no possible  $\varphi$ -phase control to a particular polarization entity by the definition of entanglement:  $|\psi\rangle = \frac{1}{\sqrt{2}}(|s\rangle_1|i\rangle_2 + |s\rangle_2|i\rangle_1)$  [19]. This definition of entanglement is the physical origin of local randomness even without the addition of P-

basis summation, as mentioned in Fig. 2. Thus, the quantum mystery of the delayed-choice quantum eraser originates in the superposition of the orthogonal bases of a physical entity, i.e., a single photon. In other words, the quantum mystery of the delayed-choice experiments in Fig. 2 for quantum eraser originates in the superposition of orthogonal bases of a photon, where the superposition requires coherence between the bases.

For the particle nature, the bases must be distinguished as provided by PBS in Fig. 1. This feature seems to be the same as that of classical particles, but the paired bases require coherence between them, as shown in Fig. 2. For the wave nature, however, the bases must be indistinguishable, where the polarizer's rotation makes the polarization bases indistinguishable. Thus, the implied coherence of the particle nature can be recovered to the wave nature by the polarizer, resulting in the fringe. In that sense, classical particles cannot be the same as quantum particles because of no coherence. For example, the SPDC-generated entangled photon pairs measured in each detector seems to be incoherent until two-photon intensity correlation is measured [22]. Due to the basis coherence, the two-photon intensity correlation between both detectors results in coherence-based fringes via measurement modification for only correlated pairs, as discussed for Franson-type nonlocal correlation [26].

## 5. Conclusion

The coherence interpretation of the delayed-choice experiments was conducted for the quantum eraser via post-control of polarization basis of the output photons. Unlike conventional delayed-choice experiments, a predetermined photon characteristic inside MZI was retrospectively converted into the wave nature via output photon's polarization-basis projection, resulting in the violation of the cause-effect relation. The quantum feature of the which-way information in an interferometer was erased without a direct control of the interferometer, where the polarization-basis projection onto a common axis is for switching the distinguishable bases to indistinguishable ones in measurements. The demonstrated post-measurement-based delayed-choice quantum eraser was interpreted for a selective choice of measurement basis, resulting in swapping between the particle and wave natures of a photon. Thus, the quantum mystery of the delayed-choice quantum eraser was understood in such a way that the coherence control of the orthonormal bases of a single photon is the origin of the quantum mystery. This understanding becomes the bedrock of the two-photon nonlocal correlation (see Appendix D) [26].

## Appendix A

Table 1 shows raw data of the left column in Fig. 2 for  $0 \leq \varphi \leq 2\pi$ . The values include five dark counts (per 0.1 s) in both D1 and D2. Only partial data points starting from  $\varphi = 0$  are displaced to verify the data points in Fig. 2. The data in Table S1 is from the recorded file by the home-made LV program.

**Table 1.** Raw data of the left column in Fig. 2.

No. data point	D1				D2				D1D2 coincidence			
	90	45	-45	0	90	45	-45	0	90	45	-45	0
181	25149	262	49274	25603	24593	49838	160	25132	89	2	2	92
182	25228	461	50002	25314	25003	49639	76	25336	91	4	1	92
183	24944	604	50294	25180	24771	49496	187	25187	89	5	2	91
184	25443	485	49485	25501	24732	49615	228	25426	90	4	2	93
185	24746	565	49283	25387	24922	49535	376	25357	89	4	3	92
186	24984	755	49255	25362	25113	49345	524	25297	90	6	4	92
187	25011	905	48813	25024	25146	49195	764	25146	90	7	6	90
188	24931	1172	48047	24954	24773	48928	772	25267	89	9	6	91
189	24840	1291	48073	25738	24874	48809	951	25367	89	10	7	94
190	25324	1596	48635	25508	24782	48504	1472	25501	90	12	11	93
191	24816	1584	48101	25131	25264	48516	1734	25273	90	11	12	91
192	25072	1783	47243	25326	25043	48317	1710	25306	90	13	12	92
193	24895	2459	47267	25362	24843	47641	2103	25590	89	17	15	93
194	24969	2583	47185	25554	25122	47517	2336	25603	90	18	16	94
195	25158	2993	47203	25273	24998	47107	2767	25069	90	21	19	91
196	24805	3374	46696	25381	24827	46726	3131	25394	88	23	21	93
197	24791	3762	46900	25292	24984	46338	3999	25183	89	25	27	91
198	24924	3888	46094	25149	25155	46212	4397	25559	90	26	29	92
199	25003	4339	45053	25171	25138	45761	4598	25035	90	29	30	91
200	25124	4821	44635	25131	25164	45279	5117	25568	91	32	33	92
201	24917	4904	43998	25517	24838	45196	5915	25015	89	32	38	92
202	25036	4863	43613	25498	24874	45237	6211	25092	89	32	39	92
203	25257	5600	43493	25445	25140	44500	6790	24973	91	36	43	91
204	24786	6647	43533	25139	24913	43453	7627	25778	89	42	48	93
205	25196	6904	42261	25401	25203	43196	8515	25263	91	43	52	92
206	25092	7530	42407	25292	25090	42570	8633	25437	90	46	53	92
207	25117	7940	41190	25248	25347	42160	9623	25364	91	48	57	92
208	25016	8498	40553	25335	25151	41602	10246	25035	90	51	60	91
209	25065	8781	40116	25272	25320	41319	10877	25284	91	52	63	92
210	24937	9805	40196	25772	25047	40295	11703	25306	90	57	68	94
211	24912	10758	39317	25460	25263	39342	12523	25146	90	61	71	92
212	24881	11342	38410	25656	24886	38758	13037	25416	89	63	72	94
⋮	⋮	⋮	⋮	⋮	⋮	⋮	⋮	⋮	⋮	⋮	⋮	⋮
360	25003	430	49840	25486	24998	49670	282	25564	90	4	3	94

Figure 6 shows Poisson distributed photon statistics obtained from an attenuated laser by using neutral density (ND) filters. With appropriate NDs, a particular mean photon number can be set, where the measurement setup and measured photon streams are shown in Figs. 6(a) and (b). In the coincidence setup in Fig. 6(a), both single photon detectors (D1 and D2) count single photons independently, as shown in Table 2 of Appendix B. The doubly bunched photons are measured by the coincidence counting module (CCU; not shown) via D1 and D2, where the oscilloscope is replaced by CCU. The box in Fig. 6(b) is to show the case of doubly bunched photons. By splitting each output path into two using a BS, four detector correlation scheme is configured (not shown) for multiply bunched photon detection, as shown in Fig. 6(c). The counted photon numbers depend on the laser intensity. From all measured counts, Fig. 6(c) shows functions for single, double, and triple photons, satisfying Poisson distribution. For all individual data measured for one second, corresponding errors (standard deviation) are also calculated ('sigma' in Table 2). From Fig. 6(c), it is clear that a less mean photon number is better to avoid bunched photons. For example, the ratio of single to double photons at 1 Mcps is  $6440/1,000,000=6.4 \times 10^{-3}$ . However, it is  $750,000/10,000,000=0.075$  for 10 Mcps. The ratio of triple to double photon ratio is similar to the single to double ratio:  $25.6/6440=3.7 \times 10^{-3}$ . Thus, the triply or higher bunched photon cases are neglected compared to the doubly bunched one.

Figure 2 is for a half million single photon case, resulting in a less than 1% bunched photon ratio. For the mean photon number calculation, the detected half million photons are divided by the dead time (22 ns)-caused time-slot numbers:  $\langle n \rangle = \frac{0.5 \times 10^6}{4.5 \times 10^7} \sim 0.01$ .

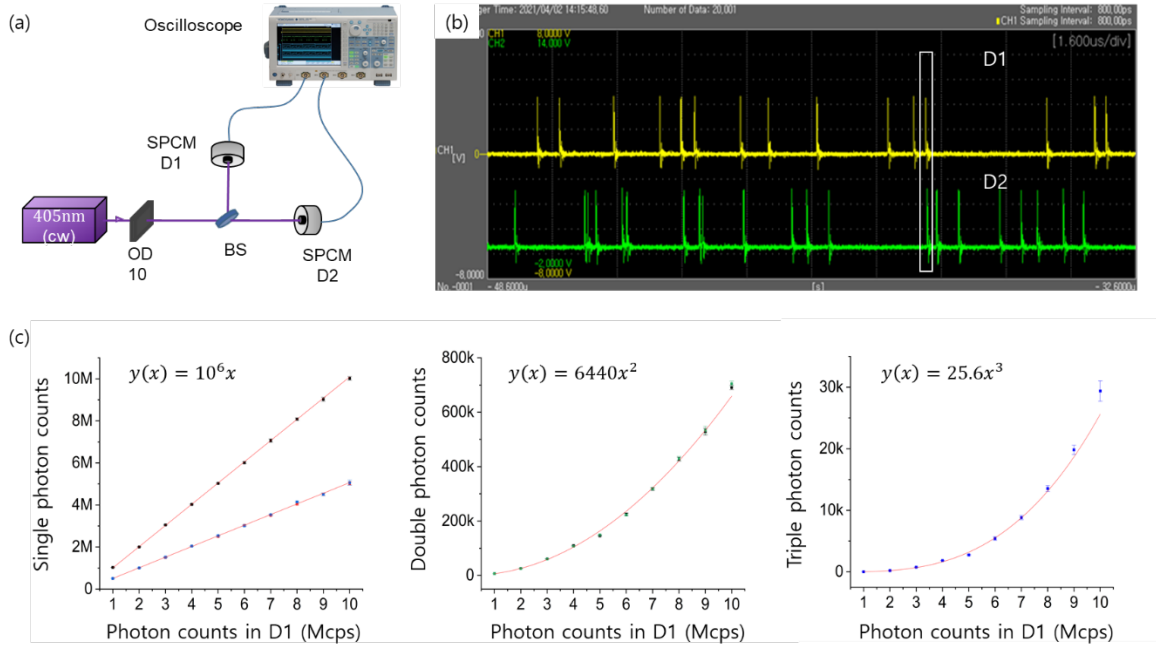


**Figure 6.** Poisson distributed photon characteristics. (a) Experimental setup for coincidence detection. (b) Single photon streams displaced on the oscilloscope. (c) Measured photon counts by CCU (see Table 2). The dots are data, and red lines are the best-fit curves.

## Appendix B

**Table 2.** Photon statistics for Figs. 2 and 4.

D1		D2		D1D2 coincidence	
mu	sigma	mu	sigma	mu	sigma
counts/0.1s					
131.2	3.6	111.5	1.6	0.0	0.0
209.7	4.9	209.9	3.8	0.0	0.0
307.6	6.9	309.1	7.0	0.0	0.1
401.1	7.9	412.5	6.1	0.0	0.1
507.9	5.3	509.4	5.7	0.0	0.1
600.9	7.2	631.6	7.8	0.0	0.0
701.1	8.7	701.1	4.4	0.1	0.1
800.7	10.2	806	8.6	0.1	0.1
908.5	13.1	907.5	12.6	0.1	0.1
1008.8	8.8	1025.9	10.2	0.2	0.1
2429	15.0	2024.5	11.5	0.6	0.1
3015.9	17.0	3030	17.4	1.4	0.4
4014.5	20.8	4099.1	22.4	2.4	0.5
5010.3	40.6	5150.3	33.8	4.2	0.4
6085.6	35.4	6041.8	35.4	5.6	0.8
7010.2	41.7	7057.7	38.3	7.2	0.3
8055.6	45.9	8080.7	41.0	9.7	0.9
9102.8	53.8	9107.1	52.0	12.6	1.0
10100.1	62.2	10103.4	59.3	15.0	1.4
20040.1	87.4	20051.9	72.0	60.9	2.4
30200	100.8	30200.1	150.8	135.1	3.7
40600.1	160.5	40350.5	115.4	242.4	5.8
50500.1	223.1	50358.1	175.8	377.8	6.3
60699.5	313.6	61086.6	245.3	554.4	6.9
72000	382.0	71120.7	249.4	753.0	9.5
82000.1	420.2	82007.9	341.6	996.7	12.5
90036.6	452.4	90002.4	389.4	1197.2	18.6
100090.5	513.9	103092.7	482.1	1578.1	25.3

Table 2 shows the measurement results for UP and LP in Fig. 1 without BS and Ps to show coherent photon statistics. In each row, the average value (mu) and standard deviation (sigma) are for 30 individual samples of recorded data, where each sample is for 0.1 s accumulation time. Table 2 follows the Poisson statistics, as shown in Fig. 6(c), where the estimated standard deviation (see the shaded row) for D1 and D2 in Fig. 2 is less than 1 %. This extremely low error rate is the benefit of the coherent photons. The coincidence measurements (right two columns) are not for single photons but for doubly-bunched photon pairs, whose generation rate is  $\sim 1\%$  of single photons.

## Appendix C

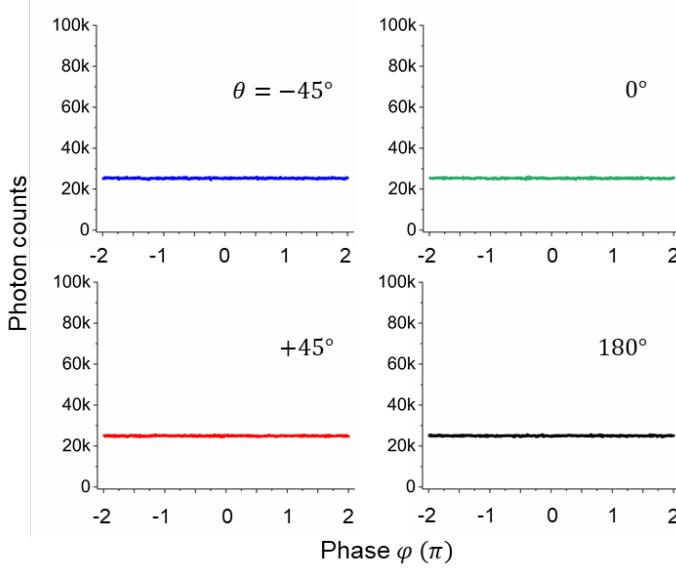


**Figure 7.** Details for the bottom panel of Fig. 2.

Figure 7 shows details of the bottom panel of Fig. 2 for all rotation angles of the polarizer P measured either detector D1 or D2. Due to incoherence between two paths of the MZI, i.e.,  $\Delta L \gg l_c$ , no interference fringe is observed, where the cosine term in Eqs. (6) and (7) drops off due to no coherence. This demonstrates that the delayed-choice quantum eraser requires coherence between superposed bases of a particle.

## Appendix D

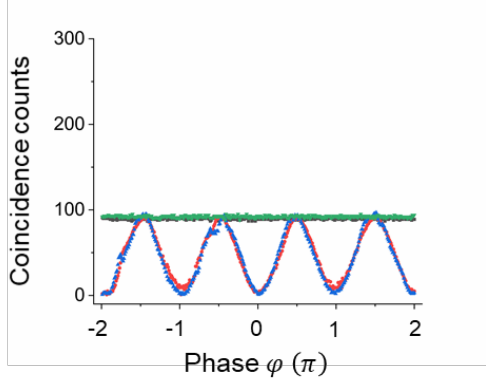


**Figure 8.** Coincidence detection for D1 and D2 in the top and middle panels of Fig. 2. Red:  $\theta = 45^\circ$ , Blue:  $\theta = -45^\circ$ , Green:  $\theta = 0^\circ$ , Black:  $\theta = 180^\circ$ .

Figure 8 shows the experimental demonstrations of coincidence detection measured by CCU for the top and middle panels of Fig. 2. The doubled oscillation frequency in Fig. 8 for  $\theta = \pm 45^\circ$  is due to the multiplication of Eqs. (6) and (7) by the definition of coincidence detection:  $I_{AB} = I_A I_B = \frac{I_0^2}{16} \sin^2 \varphi$ . As shown, the maximum coincidence counts are about 100. Compared with fifty thousands of single photon counts in Fig. 2, the generation ratio of single to double photons is definitely less than 1%.

## References

1. J. A. Wheeler, in *Mathematical Foundations of Quantum Theory*, Marlow, A. R. Ed. (Academic Press, 1978), pp. 9-48.
2. Bohr, N. in *Quantum Theory and Measurement*, J.A. Wheeler, W.H. Zurek, Eds. (Princeton Univ. Press, Princeton, NJ, 1984), pp. 9-49.
3. Scully, M. O.; Englert, B.-G.; Walther, H. "Quantum optical tests of complementarity," *Nature* **1991**, *351*, 111-116.
4. Schwindt, P. D. D.; Kwiat, P. G.; Englert, B.-G. Quantitative wave-particle duality and nonerasing quantum eraser. *Phys. Rev. A* **1999**, *60*, 4285-4290.
5. Peng, T.; Chen, H.; Shih, Y.; Scully, M. O. Delayed-choice quantum eraser with thermal light. *Phys. Rev. Lett.* **2014**, *112*, 180401.
6. Garg, A.; Mermin, N. D. Detector inefficiencies in the Einstein-Podolsky-Rosen experiment. *Phys. Rev. D* **1987**, *35*, 3831-3835.
7. Jacques, V.; Wu, E.; Grosshans, F.; Treussart, F.; Grangier, P.; Aspect, A.; Roch, J.-F. Experimental realization of Wheeler's delayed-choice Gedanken Experiment. *Science* **2007**, *315*, 966-978.
8. DuÈrr, S.; Nonn, T.; Rempe, G. Origin of quantum-mechanical complementarity probed by a 'which-way' experiment in an atom interferometer. *Nature* **1998**, *395*, 33-37.
9. Kim, Y.-H.; Yu, R.; Kulik, S. P.; Shih, Y. Delayed "Choice" Quantum Eraser. *Phys. Rev. Lett.* **1999**, *84*, 1-4.
10. Ionicioiu, R.; Jennewein, T.; Mann, R. B.; Terno, D. R. Is wave-particle objectivity compatible with determinism and locality? *Nature. Communi.* **2014**, *5*, 4997.
11. Wang, K.; Xu, Q.; Zhu, S.; Ma, X.-S. Quantum wave-particle superposition in a delayed-choice experiment," *Nature. Photon.* **2019**, *13*, 872-877.
12. Manning, A. G.; Khakimov, R. I.; Dall, R. G.; Truscott, A. G. Wheeler's delayed-choice gedanken experiment with a single atom. *Nature. Phys.* **2015**, *11*, 539-542.
13. Aharonov, Y.; Zubairy, M. S. Time and the quantum: erasing the past and impacting the future. *Science* **2005**, *307*, 875-879.
14. Ionicioiu, R.; Terno, D. R. Proposal for a quantum delayed-choice experiment. *Phys. Rev. Lett.* **2011**, *107*, 230406.
15. Dimitrova, T. L.; Weis, A. Single photon quantum erasing: a demonstration experiment. *Eur. J. Phys.* **2010**, *31*, 625.
16. Tang, J.-S.; Li, Y.-L.; Xu, X.-Y.; Xiang, G.-Y.; Li, C.-F.; Guo, G.-C. Realization of quantum Wheeler's delayed-choice experiment. *Nature. Photon.* **2012**, *6*, 600-604.
17. Ma, X.-S.; Kofler, J.; Zeilinger, A. Delayed-choice gedanken experiments and their realizations," *Rev. Mod. Phys.* **2016**, *88*, 015005.
18. Henry, M. Fresnel-Arago laws for interference in polarized light: A demonstration experiment," *Am. J. Phys.* **1981**, *49*, 690-691.
19. Herzog, T. J.; Kwiat, P. G.; Weinfurter, H.; Zeilinger, A. Complementarity and the quantum eraser. *Phys. Rev. Lett.* **1995**, *75*, 3034-3037.
20. Ham, B. S. The origin of anticorrelation for photon bunching on a beam splitter. *Sci. Rep.* **2020**, *10*, 7309.
21. Solano, E.; Matos Filho, R. L.; Zagury, N. Deterministic Bell states and measurement of motional state of two trapped ions. *Phys. Rev. A* **1999**, *59*, R2539-R2543.

22. Kim, T.; Fiorentino, M.; Wong, F. N. C. Phase-stable source of polarization-entangled photons using a polarization Sagnac interferometer," *Phys. Rev. A* **2006**, *73*, 012316.
23. Zhang, C.; Huang, Y.-F.; Liu, B.-H.; Li, C.-F.; Guo, G.-C. Spontaneous parametric down-conversion sources for multiphoton experiments. *Adv. Quantum Tech.* **2021**, *4*, 2000132.
24. Feynman, R. P.; Leighton, R.; Sands, M. *The Feynman Lectures on Physics*, Vol. III (Addison Wesley, Reading, MA, 1965).
25. Degiorgio, V. Phase shift between the transmitted and the reflected optical fields of a semireflecting lossless mirror is  $\pi/2$ . *Am. J. Phys.* **1980**, *48*, 81-82.
26. Ham, B. S. Understanding of coincidence detection in Franson-type nonlocal correlations for second-order quantum superposition. arXiv:2203.07598 (2022).

**Author Contributions:** S.K conceived the idea, conducted experiments and provided the data. B.S.H. developed the idea, analyzed the data, and wrote the manuscript.

**Funding:** This work was supported by the ICT R&D program of MSIT/IITP (No. 2021-0-01810) via Development of Elemental Technologies for ultra-secure Quantum Internet.

**Conflicts of Interest:** The author declares no conflict of interest.

**Data Availability Statement:** All results and data obtained can be found in open access publications.